Flange buckling in stainless-steel corrugated webs I-girders under pure bending: Numerical study

Journal of Constructional Steel Research 208 (2023) 108031

Contents lists available at ScienceDirect

Journal of Constructional Steel Research

journal homepage: www.elsevier.com/locate/jcsr

Flange buckling in stainless-steel corrugated webs I-girders under pure bending: Numerical study

Fatima Hlal *, Mohammad Al-Emrani

Department of Architecture and Civil Engineering, Chalmers University of Technology, Gothenburg, Sweden

ARTICLE INFO

Keywords:
Duplex stainless steel
Corrugated web
Flange buckling resistance
Trapezoidal corrugation
Bending moment resistance
Parametric study

ABSTRACT

Structural elements with corrugated webs are used in a variety of applications, including buildings and bridges. Due to the high shear strength of the corrugated web, these elements offer a material-efficient design. Among various design aspects of beams with corrugated webs, studies on the flange buckling in these beams are scarce. Previous research has shown that the EN1993–1-5 flange buckling resistance model frequently predicts unsafe resistances. Moreover, the design model in EN1993–1-5 is developed exclusively for carbon steel and not updated for stainless steel.

In this paper, an investigation into the flange buckling behaviour in duplex stainless-steel girders is provided. A parametric finite element model is developed and validated. Linear buckling analysis (LBA) and geometrically and materially nonlinear analysis with imperfections (GMNIA) are conducted using finite element analysis for 410 girders with typical bridge girders dimensions. The results are compared to previously developed models for C—Mn steel, and a new buckling curve and entire design procedure for duplex stainless-steel girders with corrugated webs are provided to account for flange buckling. The study demonstrates that the new proposed design model provides better estimations of flange buckling resistance than prior proposed models.

1. Introduction

Carbon steel corrugated web beams have been widely used in civil engineering applications such as buildings and bridges. The use of corrugated web beams in buildings dates back to the early 1960s in Europe. In bridges, corrugated web beams as bridge girders were already seen in the 1980s in Japan and Europe [1]. The reason for using these beams is that they have shown to be a cost-effective option. This is because using a corrugated web enables using thinner plates in the web without the need for vertical stiffeners, minimizing the cost of beam manufacturing while also improving fatigue life [2].

Using stainless steel material as an alternative for C—Mn steel material in corrosive environments and weight-sensitive structures such as bridge girders is now gaining popularity. In addition to offering excellent resistance to corrosion, stainless steel offers good weldability and high strength [3].

The structural behaviour of beams with corrugated webs is relatively well studied. Previous experimental and numerical studies showed that the profile of the corrugated web has a substantial impact on the distribution of axial stress in the web. Normal stress in the web diminishes rapidly at a short distance below the junction between the web and flange and is non-existent in the main part of the web [4], a phenomenon is known as “the accordion effect”. In the design of these girders, therefore, it is common to assume that only the flanges carry the bending moment, whereas the corrugated web carries the shear force [4].

Investigations on the flange buckling resistance of corrugated web beams and its impact on the bending resistance have been limited. There is no commonly accepted method for calculating the flange buckling resistance of C—Mn steel beams with corrugated webs. EN1993–1-5 suggests using the same Winter-curve based formula for trapezoidal corrugated web girders as for flat web girders (i.e., the relationship between relative slenderness and the buckling reduction factor). However, previous experimental and numerical investigations demonstrated that when the compressed flange has a cross-sectional class of 4, the model in EN1993–1-5 frequently results in unsafe resistances [5]. Moreover, C—Mn steel was used for all prior tests and established models and these models have not been updated for stainless steel.

* Corresponding author at: Department of Architecture and Civil Engineering, Chalmers University of Technology, Sven Hultins gata 6, 412 96 Gothenburg, Sweden.
E-mail address: fatima.hlal@chalmers.se (F. Hlal).

https://doi.org/10.1016/j.jcsr.2023.108031
Received 3 February 2023; Received in revised form 27 April 2023; Accepted 22 May 2023
Available online 8 June 2023

In this paper, the buckling strength of flanges in girders composed of duplex stainless steel is investigated using finite element models. Linear buckling analysis (LBA) and geometrically and materially nonlinear analysis with imperfections (GMNIA) are employed. The finite element model is validated based on the experimental and numerical investigations performed by Jager et al. [6] on girders made of C—Mn steel. In this study, duplex 1.4162 is used as this material is most common for bridge applications. As to the magnitude of initial imperfection, a value of $c_f/50$, where c_f is the larger outstand of the flange, was verified for C—Mn steel beams with corrugated webs by Jager et al. [5] following an imperfection sensitivity study. A similar sensitivity study is performed in this work for duplex 1.4162 and a justification for the use of imperfection magnitude of $c_f/50$ is established for duplex 1.4162. The linear buckling analysis is conducted to determine the buckling coefficient k_σ. After that, a parametric study using geometrically and materially nonlinear analysis with imperfections (GMNIA) is performed to investigate the relationship between the relative slenderness of the compression flange and the reduction factor. Based on the results, a new design equation for determining the buckling coefficient k_σ and a new buckling curve $\rho\,(\bar{\lambda}_p)$ are proposed to calculate the limit for cross-section class 4 and the effective width of the compressed flange in plate girders made of duplex stainless steel. The configuration of the studied girders along with various dimensions and notations used in this study is illustrated in Fig. 1.

2. Literature study

2.1. Elastic stress distribution in flanges of beams with corrugated webs

It is common to assume, in the design of beams with corrugated webs, that the moment is carried entirely by the flanges. Previous research has also showed that the flow of shear forces in the corrugated web generates transverse bending moment in the flanges, resulting in extra normal stresses [7–9]. However, there are different opinions on the impact of the additional normal stresses. EN1993–1-5 Annex D Section D.2.1 [10] specifies a reduction factor (f_T) for the bending resistance of corrugated web girders subjected to shear and bending, which depends on the flange yield strength and the maximum normal stress level caused by the transverse bending moment. The commentary document of the EN1993–1-5 [2] emphasizes that, theoretically, these transverse bending moments are essential for reasons of equilibrium, although it is debatable how crucial they are in practice. In 1997–98, Elgaaly et al. [11–13] examined the bending and shear resistance of trapezoidal corrugated web girders. Their finding was that there is no interaction between the bending and shear resistance of trapezoidal corrugated web girders. Kövesdi et al. [7] conducted numerical analyses to estimate the transverse bending moment and its effect on the load-carrying capacity of trapezoidal corrugated web girders. The authors stated that when a plastic design is used, there is no relationship between the magnitude of the transverse bending moment and the reduction in bending resistance. Elamary et al. [14] used experimental, numerical, and analytical study to examine the behaviour of corrugated web beams loaded with bending and shear on inclined and horizontal folds. The authors concluded that there is a strong relationship between the load application location and the stress distribution on the flange, i.e., applying a load to the horizontal fold increases moment capacity because the tension stress generated at the shorter outstand width of the flange reduces compression stress in the wider outstand width side and delays buckling.

2.2. Previous design models on flange buckling resistance in beams with corrugated webs

2.2.1. EN1993–1-5 model

2.2.1.1. Elastic buckling coefficient, k_σ. Design models to account for the effect of instability on the resistance of elements require the calculation of the elastic critical buckling load or stress. For plates in compression, a buckling coefficient k_σ is needed for calculating the critical buckling stress. The value of this coefficient depends on the plate loading and support conditions. For a long plate simply supported on three edges and subjected to uniform compression, the value of the buckling coefficient is 0.425 [15]. In a corrugated web beam, the inclined folds of the corrugation can provide partial support to the flange by reducing the plate aspect ratio. The EN1993–1-5 [10] model that describes the elastic buckling coefficient k_σ for flanges in I-girders with corrugated webs recognizes this additional support, as shown in Eq. (2-1), where the buckling coefficient for plate with a length (a) is modified by adding the term $\left(\frac{c_f}{a}\right)^2$. An upper limit of 0.6 is also stipulated in this model. It was believed that there are two possible scenarios in which the flange in a corrugated web beam may buckle. Buckling of the largest flange outstand is the first possible buckling mode. This buckling mode is expected to govern for webs with deep corrugations [2]. The buckling coefficient k_σ for this mode is given in "case a" in EN1993–1-5 [16] as:

$$k_{\sigma 1} = 0.43 + \left(\frac{c_f}{a}\right)^2 \tag{2-1}$$

where $a = a_1 + 2a_4$ and $c_f = \frac{b_f}{2} + \frac{a_3}{2}$ is the larger flange outstand from the toe of the weld to either free edge of the flange, see Fig. 1.

The second buckling mode is twisting the flange and rotating around its centreline. This mode was expected to govern in beams with webs having shallow corrugations [2]. The "case b" in EN1993–1-5 [10] provides the buckling coefficient k_σ for this mode as follows:

$$k_{\sigma 2} = 0.6 \; and \; \bar{b} = \frac{b_f}{2} \tag{2-2}$$

The most unfavourable situation between "case a" and "case b"

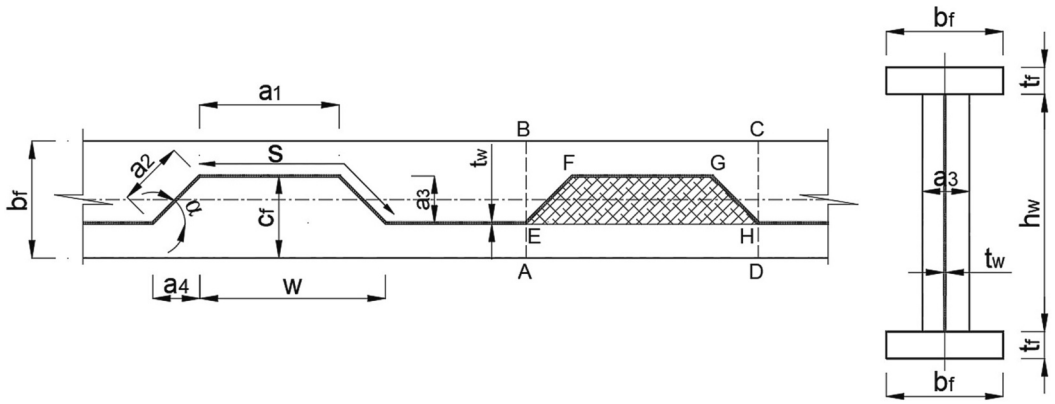

Fig. 1. Notations for beams with corrugated webs.

should be considered:

$$k_\sigma = min(k_{\sigma 1}, k_{\sigma 2}) \tag{2–3}$$

The flange plate's slenderness is then defined as:

$$\bar{\lambda}_p = \sqrt{\frac{f_y}{\sigma_{cr}}} = \frac{\frac{\bar{b}}{t}}{28.4\varepsilon\sqrt{k_\sigma}} \tag{2–4}$$

where $\varepsilon = \sqrt{\frac{235\text{MPa}}{f_y}}$, $\bar{b} = \frac{b_f}{2}$, t is the plate thickness

σ_{cr} is the critical elastic buckling stress $\sigma_{cr} = \sigma_E{}^* k_\sigma, \sigma_E = \frac{\pi^2 E t^2}{12(1-\nu^2)b^2}$

b and t are the width and the thickness the plate, ν is Poisson's ratio

2.2.1.2. Reduction buckling factor, ρ. When determining the relationship between relative slenderness $\bar{\lambda}_p$ and the buckling reduction factor ρ for flanges in trapezoidal corrugated web girders, EN1993–1-5 [10] uses the same Winter-curve based formula as for flat web girders. In section 4.4 of EN1993–1-5 [10], the reduction factor is calculated as:

$$\rho = 1.0 \, for \, \bar{\lambda}_p \leq 0.748 \tag{2-5}$$

$$\rho = \frac{\bar{\lambda}_p - 0.188}{\bar{\lambda}_p^2} \leq 1.0 \, for \, \bar{\lambda}_p > 0.748 \tag{2-6}$$

2.2.2. Model by Jager et al. [5]

2.2.2.1. Elastic buckling coefficient, k_σ. In 2017, Jager et al. [5,6] published the results of an experimental and numerical study on flange buckling in girders with corrugated webs made of C—Mn steel. The authors reported three flange failure modes to be dependent on the rigidity of the flange-to-web junction (i.e., the degree of restraint provided to the flange by the web). According to the authors, fixed support transitions to pinned support at approximately $\frac{tf}{tw} = 2.5$. The three observed failure modes were:

a. Separated local flange buckling for $\frac{tf}{tw} < 2.5$, Fig. 2 (a)
b. Combined buckling mode for $5 > \frac{tf}{tw} > 2.5$, Fig. 2 (b)
c. Flange-induced web buckling for $\frac{tf}{tw} \geq 5$,Fig. 2 (c)

Based on a large set of parametric linear buckling analyses, Jáger et al. [5] proposed a new formula for calculating the buckling coefficient for a compression flange in girders with the trapezoidal corrugated web. The model considers the aspect ratio of the plate confined within one corrugation, the enclosing effect R (defined as the ratio of areas EFGH and ABCD in Fig. 1), and the effect of the flange-to-web thickness, with an upper limit of 1.3, see Eq. 2-7.

$$k_\sigma = min\left(1.3, 0.43 \cdot \left(2.5 \cdot \frac{t_w}{t_f}\right)^{(0.6+R)} + \left(\frac{c_f}{a_1 + 2 \cdot a_4}\right)^2\right) \tag{2-7}$$

Johnson and Cafolla [17] were the first to identify the effect of the enclosing effect on the effective width due to flange buckling. Based on their experimental findings and finite element analysis, the authors determined that the average flange outstand ($b_f/2$) should be employed to calculate the relative slenderness ratio of corrugated web girders for $R <= 0.14$ and a corrugation angle of 30 degrees. For $R > 0.14$, the greater outstand c_f should be used instead.

2.2.2.2. Reduction buckling factor, ρ. To derive a buckling curve that can be used for the calculation of effective width for flanges in beams with corrugated webs, Jager et al. [5] performed parametric numerical analysis considering geometrical and materially nonlinear behaviour with imperfections. Regarding imperfection shape and amplitude, Annex C in EN1993–1-5 [10] suggests an imperfection value for the flange twist of $\frac{l}{50}$, l being the outstand length c_f. However, this value is not specific for corrugated web beams. Therefore, Jager et al. [5] conducted an imperfection sensitivity analysis to investigate the applicability of using $\frac{cf}{50}$ as the imperfection amplitude together with the 1st eigen buckling mode as the imperfection shape for corrugated web beams. The moment capacity of corrugated web girders was estimated using the numerical model developed in their work, and the findings were compared to test data for girders having flanges with various cross-sectional classes. It was concluded that an initial imperfection magnitude of $\frac{cf}{50}$ with 1st eigen buckling mode as the imperfection shape provides a satisfactory estimate for the flange buckling resistance of corrugated web girders. Based on their numerical results the authors developed a new model for the flange buckling resistance of corrugated web beams. The model can be summarized as follows:

The buckling reduction factor can be calculated as:

$$\rho_a = min\left(1, \left(14 \cdot \varepsilon \cdot \frac{t_f}{c_f}\right)^\beta\right) \tag{2-8}$$

The factor β considers the corrugation configuration and it is defined as:

$$\beta = 5 \cdot \eta \cdot R \cdot \left(\frac{1}{tan(\alpha)}\right)^\eta \tag{2-9}$$

where $0.5 \leq \beta \leq 1$

The enclosing effect can be calculated as follows:

$$R = \frac{(a_1 + a_4) \cdot a_3}{(a_1 + 2 \cdot a_4) \cdot b_f} < 0.14 \tag{2-10}$$

The factor η considers the flange to web thicknesses ratio and it is defined as follows:

$$\eta = 0.45 + 0.06 \cdot \frac{t_f}{t_w} \tag{2-11}$$

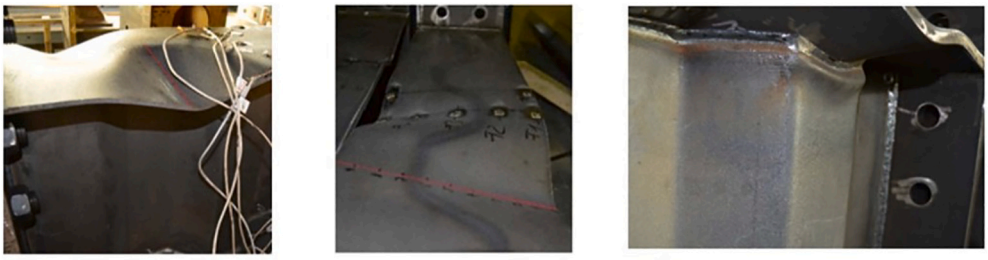

(a) (b) (c)

Fig. 2. Observed flange failure modes in Jager et al.'s experiments [6]. (a) Separated local flange buckling, (b) Combined flange buckling, (c) Flange induced web buckling.

And the larger outstand of the compression flange being:

$$c_f = \frac{b_f + a_3}{2} \tag{2-12}$$

2.2.3. DASt-Richtlinie 015 model

The DASt-Richtlinie 015 proposes a simple model which considers only the thickness and the yield strength of the compressed flange [18]. The suggested effective width for the compression flange of corrugated web girders in this model is:

$$b_{f,eff} = 30.7 \cdot t_f \cdot \sqrt{\frac{240}{f_{yf}}} \leq b_f \tag{2-13}$$

3. Numerical parametric study on duplex 1.4162

In this study, the problem of flange buckling in girders with corrugated webs made of duplex stainless steel is investigated using FE analysis. Linear buckling analysis (LBA) is used in the first step to obtain the critical elastic flange buckling stress in each studied beam. The corresponding buckling mode is then used as an initial imperfection in the subsequent geometrically and materially nonlinear analysis with imperfections (GMNIA). This analysis step provides the ultimate moment capacity for each studied girder from which the effective width of the compression flange is derived. Results from the FE analysis are then compiled and analysed to derive an appropriate model for calculating the buckling coefficient k_σ (from the LBA) and a buckling curve to calculate the reduction factor of slender flanges (from the GMNIA). The limit for cross-section class 4 for flanges in beams with corrugated webs is also derived.

3.1. Investigated parameters domains

In total, 410 beams with different geometrical properties are included in the parametric numerical analysis. The domains of the parameters investigated are chosen to represent dimensions and geometries typical for bridge girders. The flange-to-web thicknesses ratio t_f/t_w, corrugation angle α, and the enclosing effect R are the parameters previously proved to have a significant impact on the buckling and failure modes of beams with the corrugated web [5,14,19,20]. The height of the web is fixed in this study to 500 mm and the examined parameters are presented in Table 1.

The studied parameters domains result in slenderness and enclosing effect values of $c_f/t_f/\varepsilon = 7.1 - 37$ and $R = 0.085 - 0.44$

3.2. Numerical model description and validation

The FE models are constructed and analysed using ABAQUS CAE 2020. The software is compatible with Python programming language, making it suitable for parametric studies. The constructed numerical model, which is represented in Fig. 3, is comprised of a simply supported beam with a pinned support at one end and a roller support at the other. This beam is subjected to pure bending. To ensure that the outer sections respect the condition of 'a plane section remaining plane', the shell edges of the web and flanges on both ends are tied to their corresponding section master middle nodes that are positioned at the cross-section gravity centre (Node 1 and Node 2 in Fig. 3). Equal and opposite end moments are applied at these master points to load the model in pure bending. The applied boundary conditions at the master nodes are illustrated in Table 2.

Table 1
Investigated parameters ranges

Parameter	Investigated range
α [deg]	30 – 45 – 60
b_f/a_3	2 – 2.4 – 2.7 – 3 – 3.2 – 3.3 – 4 – 5 – 6 – 6.7 – 8
a_1/a_3	2 – 3 – 4
t_f/t_w	2.5 – 3.5 – 4.17 – 5 – 5.83 – 6.25 – 8.33 – 8.75 – 12.5
b_f [mm]	400 – 600 – 800 – 1000

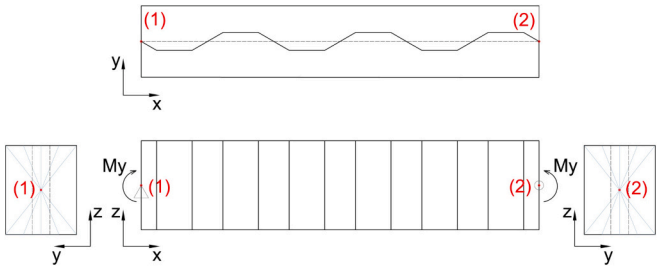

Fig. 3. Load and boundary conditions of a typical girder

To validate the FE model, the girders tested and reported by Jager et al. [6] are first modelled and analysed. These girders were made of S355 steel. Tensile tests were conducted by the authors on the steel material to register the material behaviour. An elastic-plastic with linear strain hardening material model as reported by Jager et al. [6] is implemented in this study for the finite element model validation, see Fig. 4. The yield plateau begins at the end of the linear elastic part, defined by the strain $\varepsilon_{el} = f_y/E$, and a strain of $\varepsilon = 0.01$. At a strain of $\varepsilon = 0.15$, the ultimate strength is assumed to be reached. Young's modulus is 210 GPa.

The model validation performed in this study is conducted on five selected girders (2TP1–1, 7TP1, 9TP3, 3TP1–1, 10TP4) from the experimental program reported by Jager et al. [6]. In their study, the authors tested 16 large-scale simply supported girders under four-point-bending to investigate the effect of flange buckling on the bending resistance of corrugated web beams. An illustration of the test setup is shown in Fig. 5. The central section of the beam was made up of a 1050 mm long, replaceable corrugated test specimen which was subjected to pure bending. To ensure a fixed connection, the central section was fastened to the external girder parts with bolted connections. To prevent lateral torsional buckling, the beam was supported in the lateral direction at the loading points. The nominal web height of all tested girders was 500 mm, and the total span was 8 m. The geometrical and material properties of the chosen girders for validation are summarized in Table 3.

Furthermore, in order to increase the credibility of the developed numerical model in this study, a supplementary girder (CWNCF101) tested under four-point bending by Elamary et al. [21] is included in the validation. The girder dimensions are also presented in Table 3.

The numerical model validation starts with a linear buckling analysis (LBA) and uses the first eigen buckling shape as an initial geometric imperfection in subsequent nonlinear analysis with imperfection (GMNlA). According to Jager et al. [5], an imperfection amplitude of $\frac{cf}{50}$, based on the first eigen buckling mode, can be used as an equivalent initial imperfection with adequate accuracy. Two initial imperfection amplitude values are considered during the validation process including the measured geometric imperfection from the tests, shown in Table 4, and the equivalent initial imperfection $\frac{cf}{50}$. It is important to note that residual stresses are not implicitly considered in this analysis.

To determine the most suitable mesh type and size for linear elastic buckling analysis (LBA), a mesh sensitivity study is carried out for two

Table 2
The applied boundary conditions at the master nodes (1 and 2 in Fig. 3)

	Translational degrees of freedom			Rotational degrees of freedom		
	Ux	*Uy*	*Uz*	*URx*	*URy*	*URz*
Node 1	*Fixed*	*Fixed*	*Fixed*	*Fixed*	*Free*	*Fixed*
Node 2	*Free*	*Fixed*	*Fixed*	*Fixed*	*Free*	*Fixed*

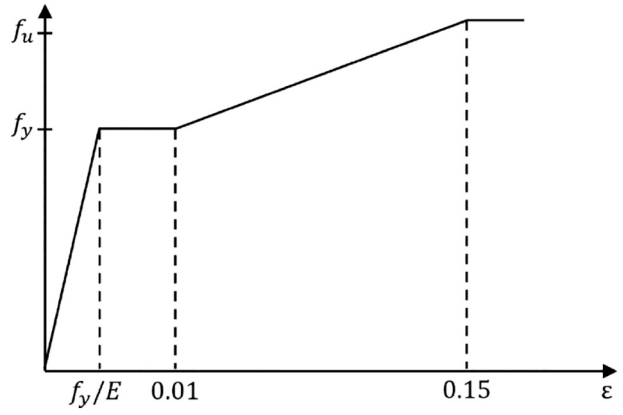

Fig. 4. Applied material model [6].

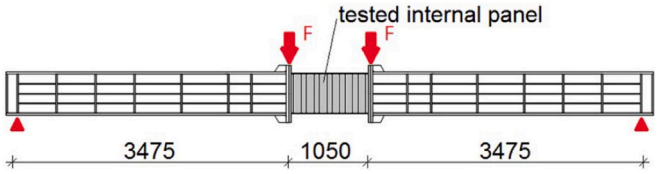

Fig. 5. Schematic drawing of the applied test arrangement [6].

mesh types, namely a four-node first-order structural element (S4R) and an eight-node second-order structural element (S8R). The mesh sensitivity study for 1st eigenvalue for one girder (9TP3) is shown in Fig. 6a. Based on the results, it turns out that the S8R mesh type reaches convergence with a coarser mesh size, thereby reducing the computation time. Consequently, the S8R mesh type is selected, and a second mesh sensitivity study is carried out for the ultimate moment capacity obtained from the nonlinear analysis, Fig. 6b.

Fig. 6 shows that the S8R mesh type with a mesh size equal to *Fold length*/4 produces satisfactory results for both buckling and nonlinear analyses. Therefore, this mesh size is selected to proceed with.

To validate the accuracy of the constructed numerical model, a nonlinear analysis is first performed on the girders listed in Table 3. The measured geometric initial imperfection, as reported by Jager et al. [6], is used in this analysis, along with the first buckling mode. The ultimate moment capacity resulting from this analysis is denoted as *Mult.num.geo*1. This moment capacityis then compared to the comparable numerical value provided by Jager et al. [5], referred to as *Mult.num.Jager.geo*1, where the authors used only the measured geometric imperfection in their validated numerical model.

Following that, a nonlinear analysis is carried out on the same girders, employing an equivalent initial imperfection of $\frac{cf}{50}$ with the first eigen buckling mode. The ultimate moment capacity obtained from this analysis is denoted as *Mult.num.geo*2. This value is also compared to the ultimate moment capacity obtained by Jager et al. [19] in their validated model, denoted as *Mult.num.Jager.geo*2, where the authors employed an equivalent initial imperfection of $\frac{cf}{50}$.

The results of the two mentioned comparisons Mult.num.geo1/Mult.num.Jager.geo1,

Mult.num.geo2/Mult.num.Jager.geo2, are shown in Table 4, which demonstrates that the finite element model results are in good agreement with the numerical findings from Jager et al. [5] [19] in both cases. The difference in results between the two sets is <3%. Additionally, there is good agreement between the ultimate moment capacity and the corresponding test findings for the girder CWNCF101, which was tested by Elamary et al. [21]. This girder is analysed using the equivalent initial imperfection ($\frac{cf}{50}$) with the first eigen buckling mode.

Finally, as the third and final step in the validation of the finite element model, data from the experiment on the relative flange displacement of girder 9TP3 is used. The effect of residual stresses was reported to be negligible in this specific girder [5], allowing for a comparison of the results obtained by employing only the measured geometrical imperfection with the test results. The relative displacement between the top and bottom flanges is calculated at CS1 and CS2, as reported by Jager et al. [6] in their work, see Fig. 7. Fig. 8 depicts the comparison between the numerical analysis results with the experimental results. Both the ultimate moment and the early stiffnesses are well-aligned, indicating a satisfactory level of accuracy of the finite element model.

The failure modes reported from the tests as well as the failure modes obtained from the nonlinear analysis are presented in Fig. 9. Girders

Table 3
Geometry of girders considered in FE model validation

Specimen	a_1 [mm]	a_3 [mm]	α [°]	t_f [mm]	b_f [mm]	t_w [mm]	h_w [mm]	f_{yf} [MPa]	f_{uf} [MPa]	f_{yw} [MPa]	f_{uw} [MPa]
2TP1–1	97	69	45	7.9	250	5.97	500	452	548	406	530
7TP1	97	69	45	12.2	250	3.84	500	364	496	474	584
9TP3	88	44	30	12.16	247	4.04	500	365	500	457	584
3TP1–1	97	69	45	14.59	250	3.01	500	387	516	363	514
10TP4	134	67	30	12.2	250	3.89	500	361	488	457	560
CWNCF101	100	50	45	4	100	2.1	400	320	390	310	390

Table 4
Validation of FE model with tests and previous numerical results.

Specimen	**2TP1 – 1**	**7TP1**	**9TP3**	**3TP1 – 1**	**4TP10**	***CWNCF*101**
Measured imperfection [mm]	1.1	1.22	1.42	1.22	1.2	Not reported
Equivalent imperfection Cf/50 [mm]	3.19	3.19	2.91	3.19	3.17	1.5
Mexp [kNm]	369	588	585	743	572	43
Mult.num.geo1	408	553	558	713	544.4	–
Mult.num.geo2	359	517.6	535	672.5	503	43.3
Mult.num.Jager.geo1	413.3	571.5	576.2	Not reported	569.9	–
Mult.num.Jager.geo2	360.4	521.2	541.9	681.5	515.2	–
Mult.num.geo1/Mexp	1.11	0.94	0.95	0.96	0.95	–
Mult.num.geo1/Mult.num.Jager.geo1	0.99	0.97	0.97	–	0.96	–
Mult.num.geo2/Mult.num.Jager.geo2	1.00	0.99	0.99	0.99	0.98	–

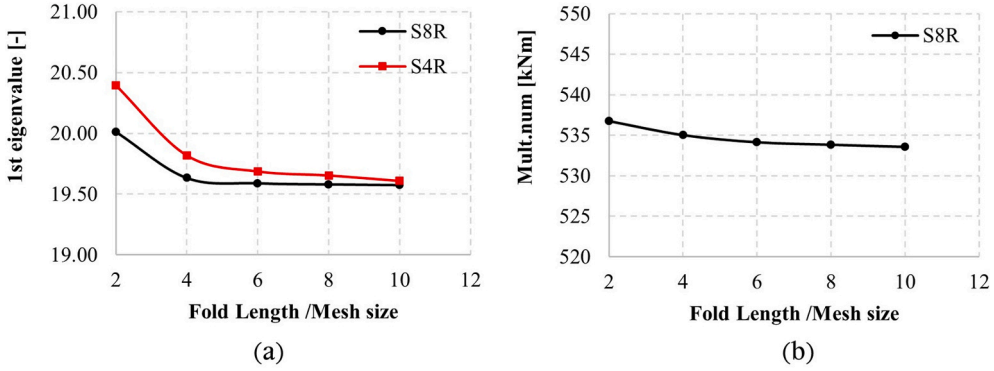

Fig. 6. Mesh sensitivity study for girder 9TP3. (a) Mesh sensitivity for 1st eigenvalue (b) Mesh sensitivity for ultimate moment capacity.

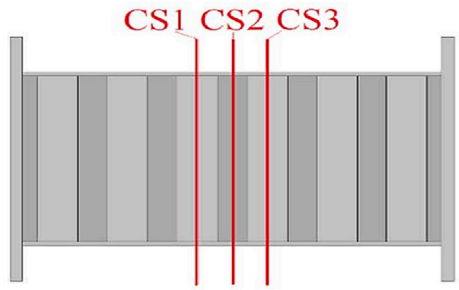

Fig. 7. CS1, CS3: cross-sections at first parallel web fold, counting from the mid-span, CS2: cross-section at mid-span. CS1 and CS2 were used to measure the relative displacement of the flanges [6].

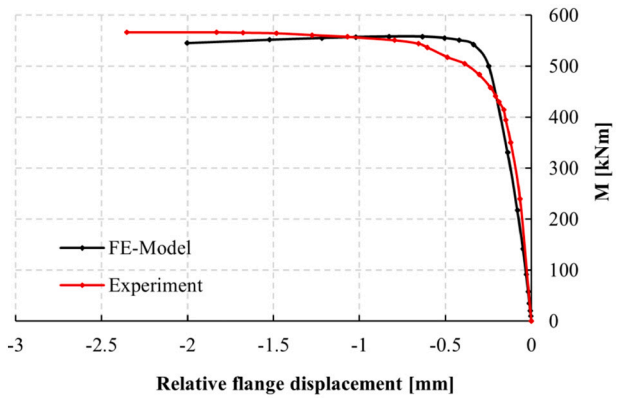

Fig. 8. Relative flange displacement obtained from the FE model and the experiment of specimen 9TP3.

9TP3, 10TP4 and 7TP1 displayed a combined buckling failure mode, however girders 2TP1–1 and CWNCF101 exhibited separate local flange buckling modes. Furthermore, girder 3TP1–1 demonstrated flange-induced web buckling.

3.3. Material model, duplex 1.4162

The material model suggested by EN1993–1-4 [22] is employed to model the material behaviour of stainless steel. The linear-elastic range and the onset of plasticity at the yield stress f_y are easily distinguished in a typical stress-strain curve for carbon steel. However, stainless steel does not have a distinct yield point. The proof stress, instead, which corresponds to a 0.2% plastic strain upon unloading, is used to determine a corresponding yield strength for stainless steels [22]. True stress-true plastic strain, stress-strain relationship for stainless steel, is employed in the implementation of the stress-strain relation in the ABAQUS. Duplex 1.4162 stainless steel is used in the parametric analysis since it is the most used stainless-steel grade in bridge applications. The material parameters are obtained from [23] and an example of the depicted material model for duplex 1.4162 plates is illustrated in Fig. 10.

3.4. Imperfection sensitivity

Before the nonlinear parametric study, an imperfection sensitivity analysis is conducted to determine an appropriate amplitude for the equivalent initial imperfection in beams made of duplex stainless steel 1.4162. Regarding the imperfection shape, the 1st eigenmode, which corresponds to flange buckling, is used. Previous studies demonstrated that the first eigenmode shape for flange buckling of trapezoidal corrugated web girders is applicable with the recommended imperfection magnitudes following the EN1993–1–5, Annex C for flange twisting for C—Mn steel [10]. However, there is no data available for stainless steel material. Therefore, a sensitivity study is conducted for the validated girders 2TP1–1, 9TP3, and 3TP1 using duplex 1.4162 material, followed by a comparison with the imperfection sensitivity curves provided by Jager et al. [5] for C—Mn steel. Fig. 11 shows an example of such a comparison. The sensitivity curves for duplex 1.4162 and C—Mn steel are similar, as can be observed, and therefore, the proposal to utilize equivalent geometric imperfection for duplex 1.4162 of a magnitude $c_f/50$ is justified.

3.5. Results of linear buckling analysis (LBA)

The elastic critical buckling moment (i.e., the moment at which bifurcation buckling of the compression flange is reached) is obtained by multiplying the applied moment in the FE model by the load amplifier obtained from the linear buckling analysis. The corresponding critical normal stress is then calculated as follows, assuming a uniform stress distribution over flange width:

$$\sigma_{cr.num} = \frac{N_{cr.num}}{b_f \cdot t_f} \; where \; N_{cr.num} = \frac{M_{cr.num}}{h_w + t_f} \tag{3-1}$$

The numerical elastic buckling coefficient is then determined from:

$$\kappa_{\sigma.num} = \frac{\sigma_{cr.num} \cdot 12 \cdot (1-\nu^2) \cdot \left(\frac{c_f}{t_f}\right)^2}{\pi^2 \cdot E} \tag{3-2}$$

where Young's modulus of stainless steel $E = 200\ GPa$ and Poisson's ratio $\nu = 0.3$

It's worth mentioning here that when analysing the results from LBA, both $\frac{b_f/2}{t_f}$ and $\frac{c_f}{t_f}$ are considered a measure of plate slenderness. It is found that the latter describes the slenderness better and results in a considerably lower scatter in the evaluation of κ_σ. Typical flange buckling shapes obtained from the linear buckling analysis are illustrated in

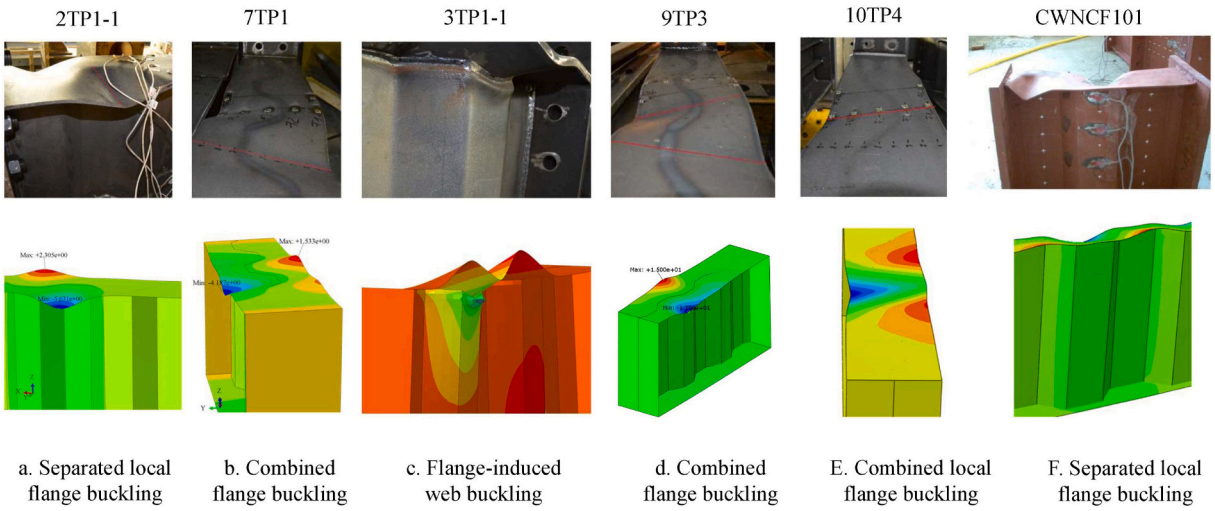

Fig. 9. Actual collapse modes versus failure modes obtained from FE analysis.

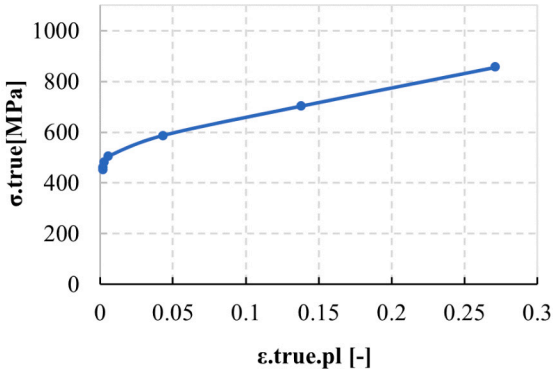

Fig. 10. An example of the material model shown for duplex 1.4162 plates with thicknesses $t > 10\,mm$.

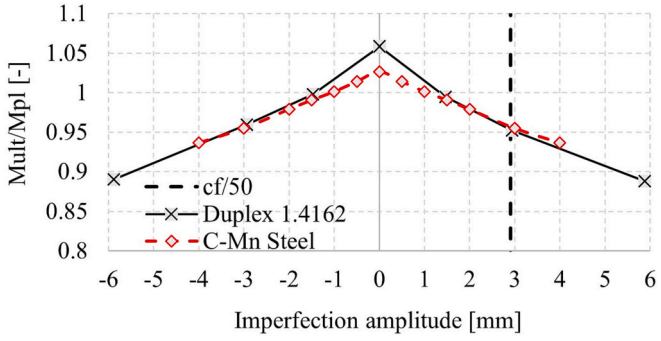

Fig. 11. Imperfection sensitivity curves for specimen 9TP3 for C—Mn steel and duplex 1.4162

Fig. 12. The general pattern for buckling modes shows that the buckling length is constrained to or within one-fold in girders with high enclosing areas (the factor R), and as the enclosing area gets smaller, the buckling length stretches across more than one-fold. This is because the corrugation provides less support to prevent buckling as the enclosing effect declines. Another mode, resembling buckling in the web is also observed as the 1st buckling mode in a few girders. This observation is particular to girders with long flat folds. Due to strain compatibility with the flanges, the web experiences axial stress in such girders, resulting - when the web is slender – in normal stress buckling in the flat fold. For these girders $\frac{t_f}{t_w}$ ranges between 5.8 and 12.5, $\frac{c_f}{t_f}$ ranges between 5 and 15 and $\frac{h_w}{t_w}$ ranges between 83 and 125. For these beams, a higher buckling mode which resembles flange buckling is used in the nonlinear analysis.

3.5.1. *Evaluation of previously proposed expressions for* κ_σ

The results obtained from the linear buckling analysis in terms of the buckling coefficient κ_σ are compared to the corresponding values proposed by EN1993–1-5 and Jager et al. [5]. The results are presented in Fig. 13. The ordinate in Fig. 13 (a) and Fig. 13 (b) represents the ratio between the buckling coefficient obtained from each model to that obtained from the linear buckling analysis conducted in this study. The abscissa represents the flange slenderness expressed as $cf/t_f/\varepsilon$.

It can be observed in Fig. 13 (a) that Eurocode's recommended formulation for the buckling coefficient κ_σ, Eq. (2–3), produces a notable dispersion with both over- and some underestimated values. It is believed that this considerable dispersion is a result of this model disregarding crucial influencing parameters such as the flange-to-web thickness ratio t_f/t_w and the enclosing effect R. The model suggested by Jager et al. [5], Section 2.2.2, performs somewhat better. The dispersion is smaller, Fig. 13 (b), and the majority of the buckling coefficients derived using Jager's model are lower than those obtained from the numerical analysis. This improvement might be a result of considering the flange-to-web thickness ratio (t_f/t_w) and the enclosing effect (R). Furthermore, Fig. 13 (c) and (d) show a comparison of the buckling coefficient obtained from both models to the numerical results obtained in this investigation. Both the models, Jager et al. [5] and the EN1993–1-5, consider upper limits for buckling coefficient of 1.3 and 0.6 respectively. However, the buckling coefficient obtained by numerical analysis ranges from 0.2 to 1.8. Consequently, neither the EN1993–1-5 model nor the model by Jager et al. [5] gives a good fit to the results obtained for girders with duplex 1.4162, and a new expression to estimate the buckling coefficient for these girders is required.

3.5.2. *The developed equation for the buckling coefficient* κ_σ

Towards the development of a new model for estimating the buckling coefficient κ_σ, four main parameters are expected to significantly influence the elastic buckling coefficient of corrugated web beams flanges. These parameters are the corrugation depth to flange width ratio $\frac{a_3}{b_f}$, the web-to-flange thicknesses ratio $\frac{t_w}{t_f}$, the flange width to flange thickness ratio $\frac{b_f}{t_f}$, and finally, the folded to unfolded lengths of one-half wave ratio $\frac{w}{s}$. The first and fourth parameters, $\frac{a_3}{b_f}$ and $\frac{w}{s}$, reflect the effect of corrugation depth and shape on the buckling length. The rotational

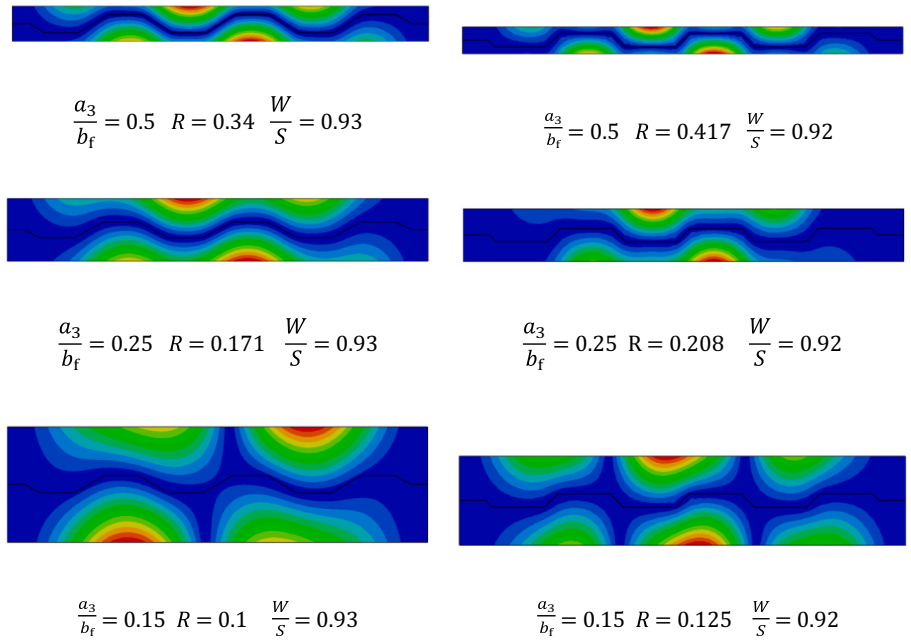

Fig. 12. Typical flange buckling modes obtained from linear buckling analysis

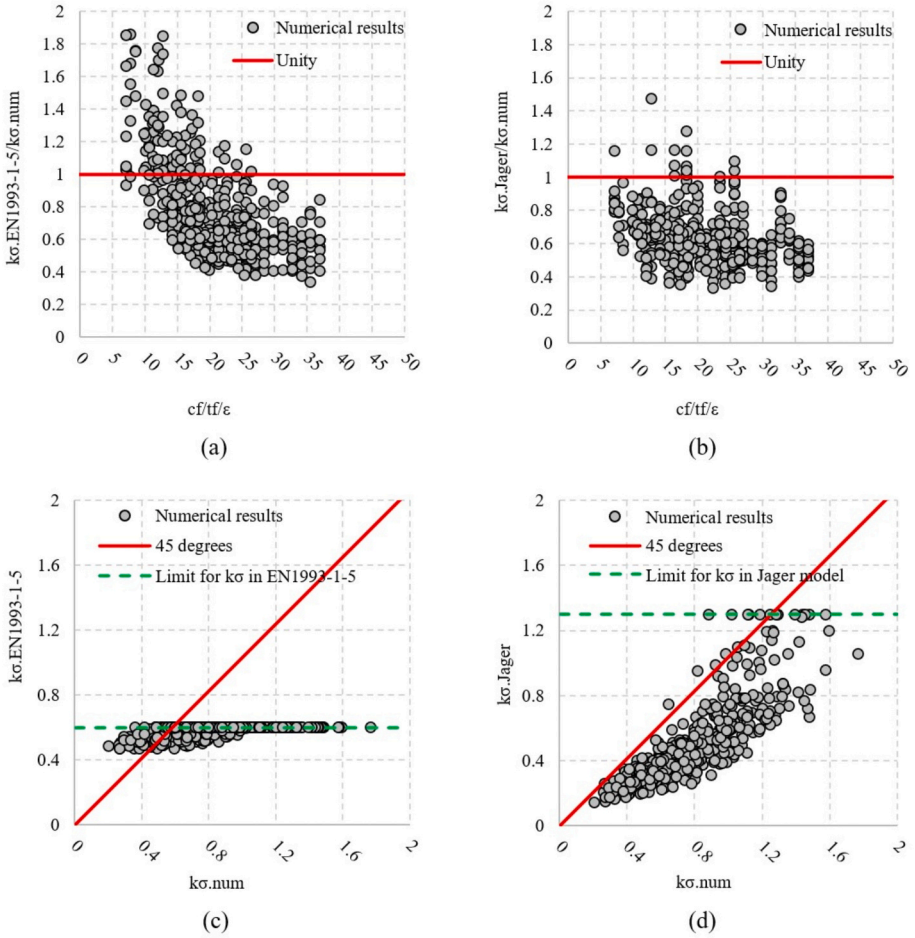

Fig. 13. A Comparison of numerical results to EN1993–1-5 and Jager et al. [5] proposals. (a) and (b) evaluate the proposals' correspondence to numerical results based on flange slenderness. (c) and (d) compare the proposals' buckling coefficients with those obtained from numerical analysis.

support provided by the web against torsion of the flange is reflected by the web-to-flange thicknesses ratio, $\frac{t_w}{t_f}$. And finally, the slenderness of the flange is determined by the ratio $\frac{b_f}{t_f}$. To fit all 410 κ_σ values obtained from the LBA to the 4 geometric parameters, a genetic algorithm optimization was employed along with a regression analysis. The resulting model is depicted in Eq. (3–3).

$$\kappa_{\sigma.corr} = 1.7 - \sqrt{\frac{a_3}{b_f}} + 0.76\cdot\frac{t_w}{t_f} + 0.94*\left(\frac{b_f}{t_f}\right)^{0.17} - 2.56\left(\frac{w}{s}\right)^2 \quad (3\text{-}3)$$

Where $w = a_1 + a_4$ and $s = a_1 + a_2$, respectively, as annotated in Fig. 1.

To evaluate the proposed model, a comparison of the buckling coefficient obtained from this proposal and the numerical results is performed and presented in Fig. 14. The derived buckling coefficient expression and the numerical outcomes demonstrate high accuracy.

Furthermore, a statistical analysis of the numerical results in comparison to the developed approximation, Eurocode approximation, and Jager approximation is presented in Table 5. As can be observed, the developed model adequately approximates the buckling coefficient in almost all 410 cases. The mean value for $\kappa_{\sigma.corr}/\kappa_{\sigma.num}$ for the proposed mode is approximately (1,0). The coefficient of variation for the developed model decreased to (CV = 9,7%) compared to (CV = 38%) for the Eurocode model and (CV = 25%) for the Jager et al. [5] model.

3.6. Results of nonlinear analysis

To construct an appropriate buckling curve for flange buckling resistance, GMNIA analyses are performed on the 410 beams included in this study. The ultimate moment capacity is obtained from the load-displacement curve, and the maximum strain is checked not to exceed 2% before the maximum moment is reached.

Fig. 15 shows typical normalized moment versus normalized rotation angle curves obtained from numerical analysis of three girders with different flange slenderness. Girder B388 with a stocky flange $\left(\frac{c_f}{t_f} = 7\varepsilon\right)$ reaches its full plastic moment and afterwards the capacity continues to increase owing to strain hardening. Girders B74 and B69 with flanges having $\left(\frac{c_f}{t_f} = 24\varepsilon\right)$ and $\left(\frac{c_f}{t_f} = 26\varepsilon\right)$, respectively, fail due to flange buckling. For the three girders indicated here, the regions that approach yielding at M_{ult} and at collapse in the post-failure stage are shown in column (b) and column (c) of Fig. 16.

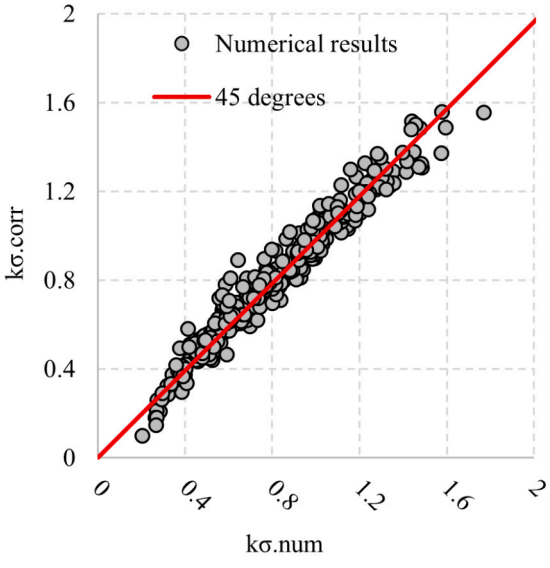

Fig. 14. Numerical results compared to the proposed expression for the buckling coefficient κ_σ

Table 5
Statistical evaluation of EN1993–1-5, Jager et al., and the proposed models

	Eurocode Model	Jager Model	Proposed Model
Average ($\kappa_{\sigma.corr}/\kappa_{\sigma.num}$)	0.81	0.63	1
Standard deviation, SD	0.31	0.16	0.097
Coefficient of variation, CV	38%	25%	9.7%

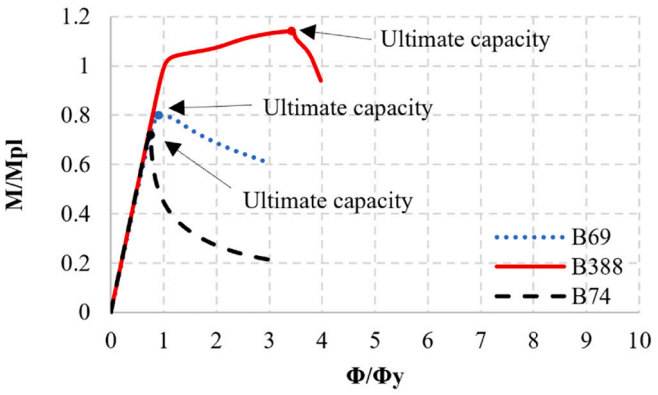

Fig. 15. Typical normalized moment versus normalized rotation angle curves obtained from numerical analysis

The results from the GMNIA analysis are processed in terms of ultimate moment resistance $M_{ult.num}$ which is obtained from the numerical analysis by multiplying the maximum load amplification factor by the applied moment. The ultimate moment resistance is then transformed to effective flange width, or buckling reduction factor, according to Eq. (3-4). Herein, any contribution from the web to the beam section modulus is neglected and the reduction factor is applied to the whole flange width b_f.

$$\rho_{num} = \frac{M_{ult.num}}{b_f\cdot t_f\cdot\left(h_{w+}t_f\right)\cdot f_{yf}} \quad (3\text{-}4)$$

Comparing the failure modes identified by Jager et al. [6] with those obtained in this study, the *separated local flange buckling mode* which was observed by Jager et al. [6] at ratios of $\frac{tf}{tw} < 2.5$, see Fig. 2a, is not observed in any of the girders analysed in this study. Bridge girders are very unlikely to have $\frac{tf}{tw}$ ratios <2.5 and therefore this value is taken as a minimum in this study. The *Flange-induced web buckling mode* which was observed by Jager et al. [6] at ratios $\frac{tf}{tw} \geq 5$, is observed in this study for some girders, but only in the post-failure phase, i.e., after the girder attains its maximum moment capacity, see Fig. 16 (B74 and B388). Adding here that this post-failure mode was observed for girders with $\frac{tf}{tw} \geq 3.5$. The last mode *combined buckling mode*, which was observed by Jager et al. [6] at ratios $5 > \frac{tf}{tw} > 2.5$, is observed as failure mode for ratios $\frac{tf}{tw} = 2.5$, see Fig. 16 (B69).

It's important to note once again that the girders that showed normal stress buckling as 1st eigen buckling mode are assigned a higher buckling mode that resembles the first flange buckling as initial imperfection (e.g., the 13th eigenmode for girder B388 in Fig. 16. Furthermore, when comparing the three different failure modes, yielding mainly occurs in the top flange or both flanges at ultimate capacity, proving the existence of the "accordion effect" for beams with corrugated web and demonstrating that the web's contribution to moment resistance is minimal for the main part of the web.

3.6.1. Evaluation of previously proposed models

The results from all 410 GMNIA analyses are used in this section to examine the appropriateness of previous models proposed for

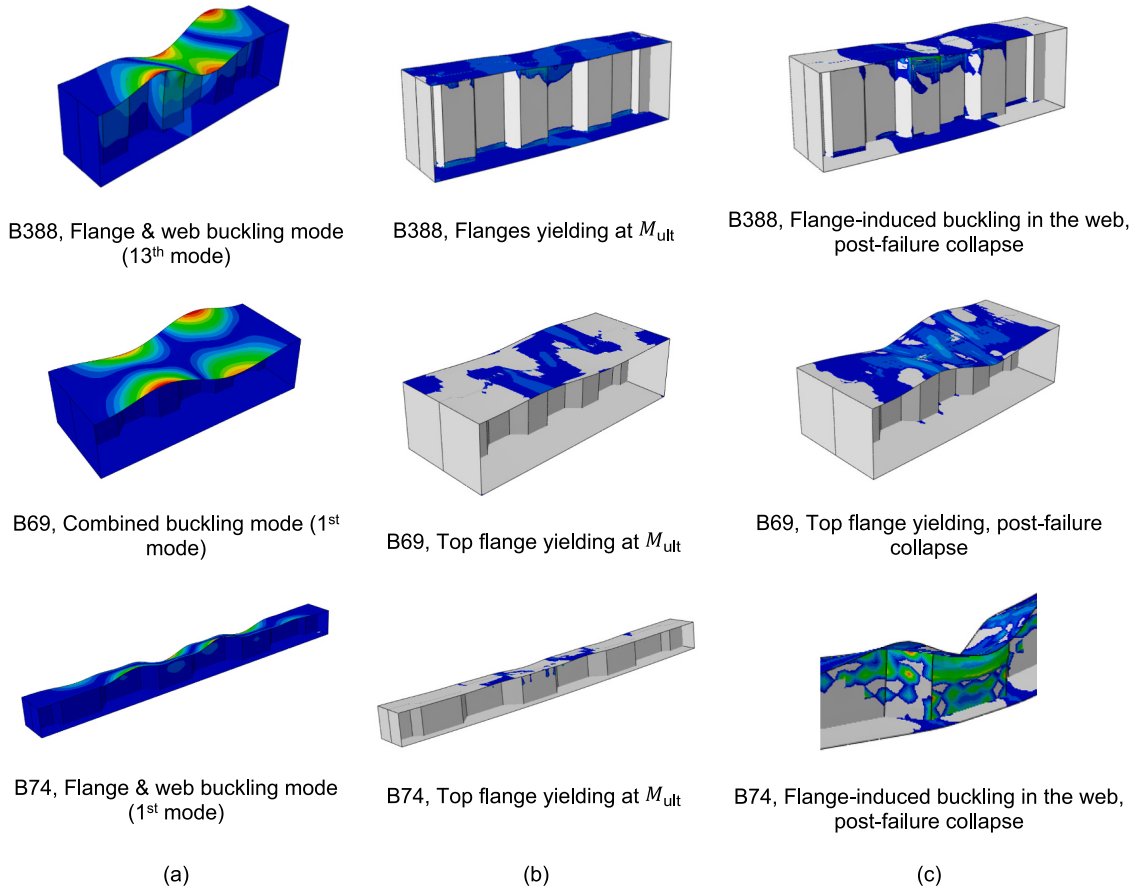

Fig. 16. (a) Buckling mode, (b) Top flange yielding at M_{ult}, (c) Post failure collapse. Coloured regions indicate yielding in the beams shown in columns (b) and (c)

calculating the flange buckling resistance in beams with corrugated webs. As mentioned before, these models were developed for beams made of C—Mn steel. The three models listed in Section 2 are considered in the comparison. The results are illustrated in Fig. 17.

The results in Fig. 17 show that the three models overestimate the bending capacities for flange buckling for duplex 1.4162. The DASt-Richtlinie 015 model, which is described in Section 2.2.3, shows the greatest dispersion. This might be attributed to the fact that this model is rather simplistic as it doesn't consider the influence of the corrugation geometry. Additionally, the EN1993–1-5 model, which is discussed in Section 2.2.1, significantly overestimates the capacities, and most of the results fall on the unsafe side. Finally, the Jager et al. [5] model, which is presented in Section 2.2.2, exhibits more relevant results compared to the EN1993–1-5 and DASt-Richtlinie 015 models. As shown in Fig. 17, the reduction factor proposed by Jager et al. [5] is calculated and applied twice: once on the large outstand c_f and once on the entire flange width b_f. Yet, the model does not demonstrate relevance to stainless steel material and the studied parameter ranges, necessitating the development of a new model.

3.6.2. Slenderness limit for cross-section class 4

To establish the slenderness limit for flanges in cross-section class 4, which determines the buckling curve's plateau length, the results of all beam simulations are plotted in Fig. 18 in terms of the slenderness ratio $c_f/t_f/\varepsilon$. The reduction factor, shown on the vertical axis, is the ratio of the plastic moment to the moment resistance determined from the numerical analysis. The relative flange slenderness, $c_f/t_f/\varepsilon$, as for a flange in a flat web girder, is used in the horizontal axis. Fig. 18 demonstrates that there is no decrease in moment capacities due to flange buckling for slenderness values of $c_f/t_f/\varepsilon < 8{,}5$. The limit for cross section class 4 might be conservatively taken as ($c_f/t_f > 8{,}5\ \varepsilon$).

Given that the flat web's buckling coefficient is constant ($k_{\sigma\_Flat} = 0.43$), the relative slenderness depends on the values of b_f, t_f, and ε. The buckling coefficient for a flange in a corrugated web beam, on the other hand, is a function of the corrugation parameters and thus is not a constant. Therefore, the results in Fig. 18 are reproduced in Fig. 19 with a definition of the slenderness limit that includes the buckling coefficient k_σ from Eq. (3-3). The limit for cross section class 4 would then be $c_f/t_f > 11.36\varepsilon^*\sqrt{k_\sigma}$. Comparing Fig. 18 to Fig. 19, it is obvious that including k_σ in the slenderness results in a more accurate estimation of CSC4 limit with substantially reduced scatter.

3.6.3. Proposed buckling curve

The evaluation of the earlier-developed models shows that these models are inadequate to accurately predict the ultimate moment capacity of duplex 1.4162 beams. Additionally, the plate buckling curve proposed by EN1993–1-5 is inappropriate for corrugated web girders made of duplex stainless steel and needs, thus, to be modified. A new model is developed in this study based on the relative slenderness ratio $\bar{\lambda}_p$ proposed in the EN1993–1-5 using the large flange outstand c_f. The primary distinction is that the predicted elastic buckling coefficient $\kappa_{\sigma.corr}$ was calculated based on the model developed in this work for the buckling coefficient, Eq. (3-3). The use of $\kappa_{\sigma.corr}$ results in small dispersion and a strong correlation between the buckling reduction factor ρ_{num} and the relative slenderness $\bar{\lambda}_p(\kappa_{\sigma.corr})$. The developed flange buckling curve is presented in Fig. 20 and the equation that describes the proposed model is defined as follows:

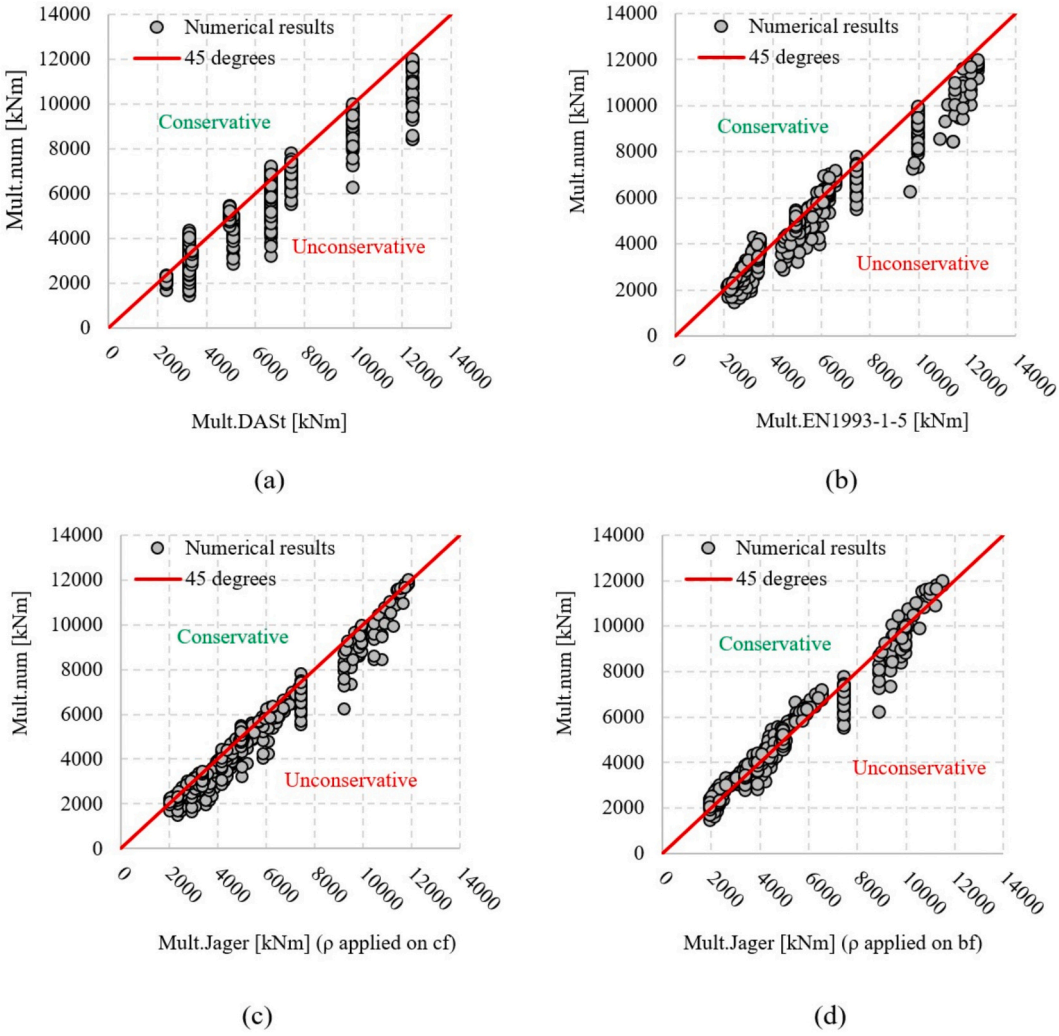

Fig. 17. Comparison of previous models based on numerical results

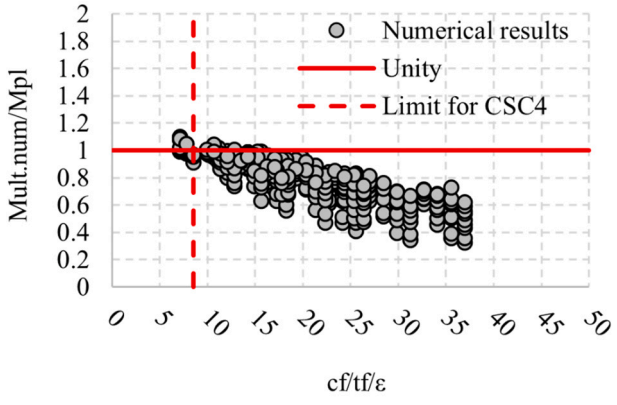

Fig. 18. M_{ult_num}/M_{pl} versus flange slenderness defined as $c_f/t_f/\varepsilon$

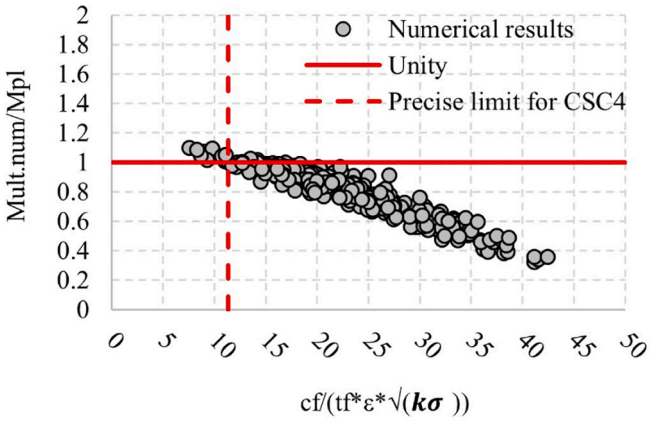

Fig. 19. M_{ult_num}/M_{pl}versus flange slenderness defined as $c_f/t_f/\varepsilon/\sqrt{k_\sigma}$

$$\rho_{corr} = 1.0 \quad \text{for } \bar{\lambda}_p \le 0.4$$
$$\rho_{corr} = \frac{0.69}{\bar{\lambda}_p} - \frac{0.1}{\bar{\lambda}_p^{\,2}} - 0.1 \le 1.0 \quad \text{for } \bar{\lambda}_p > 0.4 \tag{3–5}$$

Comparing the capacities obtained from the numerical analysis and the capacities obtained from the proposed buckling curve, Fig. 21 shows that the design model predicts the ultimate capacity with good approximation. Adding here that to get a buckling curve where all predicted capacities are on the safe side, some girders' capacities will be underestimated.

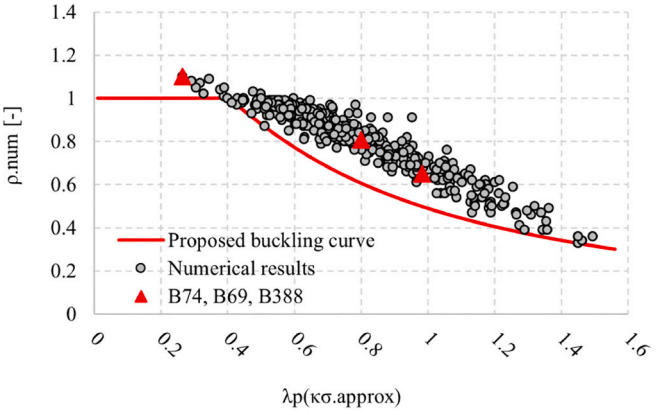

Fig. 20. Developed buckling curve for flanges in duplex corrugated web beams

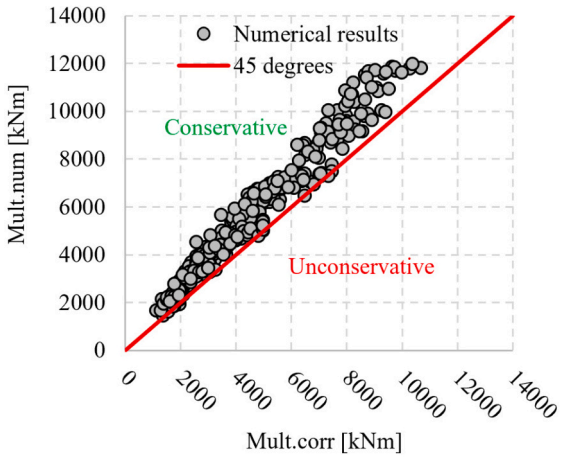

Fig. 21. Numerical results versus the approximated capacities based on the developed model

4. Proposed design procedure

The model that accounts for flange buckling in beams with trapezoidal corrugated webs made of duplex stainless steel is summarized in the following steps:

Define the limit for cross-section class 4 as follows:

if $c_f/t_f > 11.36\varepsilon^*\sqrt{k_\sigma}$ ➔ the flange is in CSC4

where the buckling coefficient is defined as:

$$\kappa_{\sigma.corr} = 1.7 - \sqrt{\frac{a_3}{b_f}} + 0.76\cdot\frac{t_w}{t_f} + 0.94\left(\frac{b_f}{t_f}\right)^{0.17} - 2.56\left(\frac{w}{s}\right)^2$$

When the flange is in CSC4, calculate the flange's relative slenderness as follows:

$$\bar{\lambda}_p = \sqrt{\frac{f_y}{\sigma_{cr}}} = \frac{c_f/tf}{28.4\varepsilon\sqrt{\kappa_{\sigma.corr}}}$$

Determine the buckling reduction factor from the following equation:

$$\rho_{corr} = 1.0 \qquad \text{for } \bar{\lambda}_p \le 0.4$$

$$\rho_{corr} = \frac{0.69}{\bar{\lambda}_p} - \frac{0.1}{\bar{\lambda}_p^{\,2}} - 0.1 \le 1.0 \qquad \text{for } \bar{\lambda}_p > 0.4$$

The moment capacity for flange buckling can now be obtained from:

$$M_{ult.Corr} = \rho_{corr}.b_f\cdot t_f\cdot\left(h_{w+}t_f\right)\cdot f_{yf}$$

5. Summary and conclusions

This paper has reported the results of an extensive numerical study on the flange buckling resistance of stainless-steel corrugated web girders. Experimental and numerical studies on carbon steel conducted by Jager et al. [6] and Elamary et al. [21] provided a foundation for the validation of the FE model. Two types of parametric numerical analyses are conducted: linear buckling analysis to estimate the elastic buckling coefficient κ_σ and nonlinear buckling analysis that considered nonlinearities in both geometry and material to develop a new buckling curve $\rho\,(\bar{\lambda}_p)$. Equivalent initial imperfections of amplitude $\frac{c_f}{50}$ and a shape of the 1st flange buckling mode is used following an imperfection sensitivity study. Three previous models: EN1993–1-5, DASt-Richtlinie 015 [18], and Jager et al. [5] are all examined in view of the produced numerical results. The following conclusions are drawn:

a. The three available models for flange buckling resistance of corrugated web girders made of C—Mn steel: EN1993–1-5, DASt-Richtlinie 015 [18], and the model proposed by Jager et al. [5], are nonconservative for duplex 1.4162 trapezoidal corrugated web girders. Both the elastic buckling coefficient κ_σ and the buckling reduction factor ρ produced by these models is unsatisfactory. The model proposed in EN1993–1-5 does not consider the rigidity of the web-to-flange junction, which has shown to be an important influential parameter. The DASt-Richtlinie 015 model does not consider the corrugation geometry. The model proposed by Jager et al. shows enhanced results since it considers both the web-to-flange junction rigidity and the corrugation geometry, however, the model results in capacities that are on the unsafe side for many girders.
b. The proposed formula for calculating the elastic buckling coefficient $k_{\sigma.corr}$, which is proposed based on the LBA of 410 plate girders with a wide range of corrugation geometries and web-to-flange thickness ratios in a domain relevant to bridge girders, provides substantially better estimations than do previously proposed models for C—Mn girders.
c. The results of the imperfection sensitivity study indicates that the 1st eigen buckling mode with imperfection amplitude of $c_f/50$, as recommended by EN1993–1-5 for flange twisting, is appropriate for flange buckling in corrugated web beams made of duplex 1.4162.
d. Three failure modes for flange buckling are observed in this study: flange-induced web buckling, combined buckling mode and separated local flange buckling.
e. The proposed buckling curve $\rho\,(\bar{\lambda}_p)$, which is based on the correlation between the relative slenderness ratio $\bar{\lambda}_p(k_{\sigma.corr})$ and the reduction buckling factor $\rho\,(\bar{\lambda}_p)$, is found to produce good results for all observed failure modes. However, owing to the complexity of the problem and many influencing parameters, a certain underestimation in the flange buckling resistance is accepted.
f. The relative slenderness limit for duplex trapezoidal corrugated web beams is $\bar{\lambda}_p \le 0.4$. This results in a cross-section class 4 limit of $c_f/t_f > 11.36\varepsilon^*\sqrt{k_\sigma}$.

The design model proposed in this research is developed specifically for the duplex stainless steel 1.4162 grade and it is based on the parameters' ranges specified in Section 3.1. Further investigation on the model's applicability for C—Mn steel and other grades of stainless steel, as well as possibly broader parameter domains, is necessary.

Authorship statement

Fatima Hlal: Methodology, Scripting, Investigation, Numerical analysis, Validation, Data curation, original draft preparation.

Mohammad Al-Emrani: Conceptualization, Supervision, Data curation, reviewing and editing, Funding acquisition.

Declaration of Competing Interest

The authors declare that they have no known competing financial interests or personal relationships that could have appeared to influence the work reported in this paper.

Data availability

Data will be made available on request.

Acknowledgement

This research was conducted as part of the "Sustainable and Maintenance free bridges" project, which was funded by the Swedish Transport Administration [Project No. TRV 2020/117504]. The financial support is gratefully acknowledged.

References

[1] H.H. Abbas, R. Sause, R.G. Driver, Behavior of corrugated web I-girders under in-plane loads, J. Eng. Mech. (2006) 806–814, https://doi.org/10.1061/(ASCE)0733-9399(2006)132:8(806).
[2] B. Johansson, G. Sedlacek, C. Müller, D. Beg, Commentary and Worked Examples to EN 1993–1-5 Plated Structural Elements. https://publications.jrc.ec.europa.eu/repository/handle/JRC38239, 2007.
[3] ISSF, The Stainless-Steel Family: International Staineless Steel Forum. https://www.worldstainless.org/Files/issf/non-image-files/PDF/TheStainlessSteelFamily.pdf, 2019.
[4] B. Kövesdi, B. Jáger, L. Dunai, Bending and shear interaction behavior of girders with trapezoidally corrugated webs, J. Constr. Steel Res. (2016), https://doi.org/10.1016/j.jcsr.2016.03.002. 121: p. 383-397.
[5] B. Jáger, L. Dunai, B. Kövesdi, Flange buckling behavior of girders with corrugated web part II: numerical study and design method development, in: Thin-Walled Structures, 2017, pp. 238–252, https://doi.org/10.1016/j.tws.2017.05.020.
[6] B. Jáger, L. Dunai, B. Kövesdi, Flange buckling behavior of girders with corrugated web part I: experimental study, in: Thin-Walled Structures, 2017, pp. 181–195, https://doi.org/10.1016/j.tws.2017.05.021.
[7] B. Kövesdi, B. Jáger, L. Dunai, Bending and shear interaction behavior of girders with trapezoidally corrugated webs, J. Constr. Steel Res. (2016) 383–397, https://doi.org/10.1016/j.jcsr.2016.03.002.
[8] B. Kövesdi, B. Jáger, L. Dunai, Stress Distribution in the Flanges of Girders with Corrugated Webs, 2012, https://doi.org/10.1016/j.jcsr.2012.07.023.
[9] H.H. Abbas, R. Sause, R.G. Driver, Analysis of flange transverse bending of corrugated web I-girders under in-plane loads, J. Struct. Eng. (2007) 347–355, https://doi.org/10.1061/(ASCE)0733-9445(2007)133:3(347).
[10] EN1993-1-5 (2006).
[11] M. Elgaaly, A. Seshadri, Depicting the Behavior of Girders with Corrugated Webs up to Failure Using Non-Linear Finite Element Analysis, 1998, https://doi.org/10.1016/S0965-9978(98)00020-9.
[12] M. Elgaaly, Bending strength of steel beams with corrugated webs, J. Struct. Eng. (1997), https://doi.org/10.1061/(ASCE)0733-9445(1997)123:6(772).
[13] M. Elgaaly, H.R. W, S. Anand, Shear strength of beams with corrugated webs, J. Struct. Eng. (1996), https://doi.org/10.1061/(ASCE)0733-9445(1996)122:4(390.
[14] A.S. Elamary, Yasir M. Alharthi, Mostafa F. Hassanein, Ibrahim A. Sharaky, Trapezoidally Corrugated Web Steel Beams loaded over Horizontal and Inclined Folds, 2022, https://doi.org/10.1016/j.jcsr.2022.107202.
[15] M. Al-Emrani, B. ÅKESSON., Steel Structures Report ACE2030:13, Department of Architecture and Civil Engineering, Chalmers University of Technology, 2020. http://bit.ly/3H3T3tv.
[16] EN1993–1-5 (2006).
[17] R.P. Johnson, J. Cafolla, Local Flange Buckling in Plate Girders with Corrugated Webs, 1997, https://doi.org/10.1680/istbu.1997.29304.
[18] H. Pasternak, D. Hannebauer, Träger mit profilierten Stegen. https://www.researchgate.net/publication/342644235, 2004.
[19] B. Jáger, B. Kövesdi, L. Dunai, Flange buckling resistance of trapezoidal web girders: experimental and numerical study, EUROSTEEL (2017), https://doi.org/10.1002/cepa.465, 4088-4097.
[20] Q. Inaam, A. Upadhyay, Accordion effect in bridge girders with corrugated webs, J. Constr. Steel Res. (2022), https://doi.org/10.1016/j.jcsr.2021.107040.
[21] A.S. Elamary, A.B. Saddek, M. Alwetaish, Effect of corrugated web on flexural capacity of steel beams, International Journal of Applied Engineering Research 12 (4) (2017) 470–481. ISSN 0973-4562.
[22] EN1993–1-4 (2006).
[23] SS-EN1993-1-4:2006/A1, Design of Steel Structures – Part 1–4: General Rules – Supplementary Rules for Stainless Steels, 2015.